CASI

FINAL REPORT
Grant No. NAG-1-1678
January 30, 1995 – December 31, 1998

TECHNOLOGY FOR ELEVATED TEMPERATURE TESTS OF STRUCTURAL PANELS

Submitted to:

Ms. Panice H. Clark, Grants Officer
National Aeronautics and Space Administration
Langley Research Center
Acquisition Division
Hampton, VA 23681-0001

Submitted by:

E. A. Thornton
Professor Emeritus

SEAS Report No. UVA/528515/MAE00/101
July 1999

DEPARTMENT OF MECHANICAL AND AEROSPACE ENGINEERING

SCHOOL OF
ENGINEERING & APPLIED SCIENCE

University of Virginia
Thornton Hall
Charlottesville, VA 22903

UNIVERSITY OF VIRGINIA
School of Engineering and Applied Science

The University of Virginia's School of Engineering and Applied Science has an undergraduate enrollment of approximately 1,500 students with a graduate enrollment of approximately 600. There are 160 faculty members, a majority of whom conduct research in addition to teaching.

Research is a vital part of the educational program and interests parallel academic specialties. These range from the classical engineering disciplines of Chemical, Civil, Electrical, and Mechanical and Aerospace to newer, more specialized fields of Applied Mechanics, Biomedical Engineering, Systems Engineering, Materials Science, Nuclear Engineering and Engineering Physics, Applied Mathematics and Computer Science. Within these disciplines there are well equipped laboratories for conducting highly specialized research. All departments offer the doctorate; Biomedical and Materials Science grant only graduate degrees. In addition, courses in the humanities are offered within the School.

The University of Virginia (which includes approximately 2,000 faculty and a total of full-time student enrollment of about 17,000), also offers professional degrees under the schools of Architecture, Law, Medicine, Nursing, Commerce, Business Administration, and Education. In addition, the College of Arts and Sciences houses departments of Mathematics, Phyics, Chemistry and others relevant to the engineering research program. The School of Engineering and Applied Science is an integral part of this University community which provides opportunities for interdisciplinary work in pursuit of the basic goals of education, research, and public service.

Technology for Elevated Temperature Tests

Abstract

A technique for full-field measurement of surface temperature and in-plane strain using a single grid imaging technique was demonstrated on a sample subjected to thermally-induced strain. The technique is based on digital imaging of a sample marked by an alternating line array of $La_2O_2S:Eu^{+3}$ thermographic phosphor and chromium illuminated by a UV lamp. Digital images of this array in unstrained and strained states were processed using a modified spin filter. Normal strain distribution was determined by combining unstrained and strained grid images using a single grid digital moiré technique. Temperature distribution was determined by ratioing images of phosphor intensity at two wavelengths. Combined strain and temperature measurements demonstrated on the thermally heated sample were $\Delta\varepsilon = \pm 250\ \mu\varepsilon$ and $\Delta T = \pm 5$ K respectively with a spatial resolution of 0.8 mm.

Introduction

Non-intrusive strain and temperature measurements are desirable for thermo-mechanical testing of structural materials, particularly newly developed high temperature composites, testing of aerodynamic models in high speed flows, and measurements in other hostile environments where thermal and strain gradients may coexist. For elevated temperature measurements, resistive strain gauges and thermocouples are most frequently employed. Although resistive strain gauges are under development for high temperature applications, generally their range of application has been below 1,000 K. Both require electrical connections and provide only pointwise measurement.

Infrared pyrometry measurements of emission from test objects is frequently used for non-contact temperature measurements. However, its dependence on the surface emissivity and spectral characteristics of the object and the effect of the temperature of the surroundings on the measurement limit the use of this technique. Alternatively, temperature measurements by resonance optical techniques, similar to laser induced fluorescence, may circumvent many of these difficulties. For temperature measurement, the surface is coated with a temperature sensitive thermographic phosphor and is illuminated by radiation that induces its excitation. The subsequent phosphorescence is imaged and interpreted to provide the distribution of the surface temperature.

Moiré interference is widely used to obtain measurements of surface strain. A typical moiré experiment uses a line array marked on a surface and a similar reference array. Interference patterns are developed by overlaying surface and reference arrays. Straining of the surface array results in changes to the interference pattern that can be related to strain using simple geometric relationships.

Thermographic phosphor temperature measurements and moiré strain measurements can be combined on a single surface by superimposing a non-phosphorescing grid on a surface coated with thermographic phosphor. The resulting surface coating when illuminated with light appropriate for exciting the thermographic phosphor, can be used to obtain high contrast images containing array pattern and thermographic phosphor intensity distributions. Processing of these images can be used to obtain both the strain and temperature distribution. A single grid digital imaging technique with potential for measuring strain and temperature distributions at elevated temperature has previously been demonstrated[1]. The technique was based on imaging a surface marked by a 5 line/mm array of thermographic phosphor established by removing lines from a

uniformly coated surface using laser etching. Due to the crystalline morphology of the thermographic phosphor, definition of edges was generally poor. The generation of phosphor arrays has been significantly improved in the current study by altering the method of array generation. For the current study, a 10 line/mm array was established by coating a thermographic phosphor with a thin layer ($\approx$0.1 μm) of chromium by evaporation. Chromium lines were removed from this surface by photolithography and etching using a 10 line/mm mask. The resulting alternating line arrays of thermographic phosphor and chromium were well-defined and uniformly spaced.

The digital moiré technique has been further enhanced by modifying the digital processing of images of the array that were used to obtain surface strain and temperature by incorporating a spin filter modified to remove extraneous pixels from the process, resulting in overall improvement in the use of these images to obtain strain and temperature.

Single Grid Digital Moiré Technique

Moiré interferometry is an optical technique widely used for visualization and measurement of the planar distribution of two dimensional strains using relatively simple equipment. The moiré pattern is a real visual–effect obtained by overlaying two grids. The resulting pattern includes, in addition to the fundamental pitch, p, of each grid, a beat–frequency component. This beat frequency can be highly sensitive to the translation, rotation or distortion of any one of the grids and therefore can be used for the imaging and measurement of distortions. In a typical moiré analysis, two line arrays, or grids, are overlaid to form a pattern of alternately bright and dark fringes. Depending on the mode of application, these fringe patterns can then be used to measure various components of mechanical strain[2], or out-of-plane displacements[3]. Usually moiré patterns are recorded photographically[4] but with the advent of digital imaging,

simpler and more powerful moiré techniques have become available[5,6]. Most of these digital techniques use a grid of parallel lines which are etched into the sample surface. The second grid, or the reference grating, can be placed between the camera and the sample surface or may be projected directly onto the surface. Thus, by viewing the object through a reference grid the moiré fringes can be viewed even if the camera resolution is insufficient to resolve the individual grating lines.

With the development of high resolution digital imaging, this entire process can be digitized and automated. Further, a single grid technique can be developed by recording images of a reference grid before a sample is subjected to external loading or heating. Subsequent images of the heated or loaded sample can then be overlaid digitally with previously recorded images of the unstrained (or reference) grid. However, because the moiré pattern is formed from images of the grids, the individual features of the grids must be resolved. Usually, grids are oriented parallel to each other and spatial and strain resolution are achieved by the use of arrays with high line density. However, the resolution achievable with digital cameras (typically 1,024 x 1,024 pixels) limits the total number of line pairs that can be recorded in a single image to approximately 250. Moiré patterns formed by parallel overlaying of grid images containing such a limited number of line pairs will be of little use in practical strain measurements. Thus, an alternative method of generating moiré patterns must be employed.

Spatial and strain resolution can be enhanced by introducing a relative rotation between the grids prior to overlaying their images. Figure 1 illustrates the interaction between the lines of two identical grids oriented at a relative angle 2θ. Inspection of this figure shows that bright fringes oriented at an angle θ, relative to the normal to either grid pattern, form along the short diagonals of the rhombus patterns enclosed by the lines of the grids. This pattern is observed even when the object is unstrained and its density may be controlled by selecting 2θ to enhance resolution.

To illustrate the effect of the distortion of one grid on the moiré fringe pattern, assume that one grid is stretched uniformly by normal strain, i.e. the line spacing is increased by dp, while the second grid is left undisturbed. This is illustrated in Figure 2 where line kk' is replaced by the dashed line. As a result, the moiré fringes pass through the diagonals of the new rhombi, e.g., $B'D$, and they appear to be inclined relative to the previous fringes, e.g. BD, by an angle γ. Using simple geometrical analysis it can be shown that:

$$\varepsilon = \frac{2}{\cot\theta \cot\gamma - 1} \tag{1}$$

where $\varepsilon = dp/p$ is the normal strain associated with the uniform stretch of the grating. No approximations were necessary to derive this equation. However, in most applications, both θ and γ are sufficiently small so that cot $\theta >> 1$ and cot $\gamma >> 1$ and the following simplified equation can be used:

$$\tan\gamma \approx \frac{\varepsilon}{2\tan\theta} \tag{2}$$

From measurement of the distribution of γ, the normal strain distribution in the imaged field can be determined.

To remove the influence of grid or imaging system distortion on measurement of fringe rotation angle γ, a reference moiré image is generated. This moiré image is obtained by overlaying two images of the unstrained array that have also been rotated by a relative angle 2θ. The actual fringe rotation angle due to strain is then obtained relative to the fringe angle determined from this reference moiré pattern.

When the strain field is dominated by shear strain, the distortion is dominated by rotation of the strained grid. Thus, the overlap between the distorted grating and the reference grating results in the following variation of the fringe spacing a_f while the fringe orientation remains

nearly unchanged:

$$a_f = \frac{p}{2\sin\theta} \tag{3}$$

An estimate of the limiting resolution of the technique can be obtained using Equations 2 and 3. In the current study, p = 10 lines/mm and an image rotation angle of $2\theta = 4$ was used. Thus fringe spacing a_f = 1.43 mm. Spatial and strain resolutions are interrelated by the dimensions required to achieve a specific resolution on fringe rotation angle γ. For example, a 1024 x 1024 pixel camera was used to image a 12.7 mm x 12.7 mm area in this study. If the required strain resolution is 250 με, then spatial resolution is predicted to be 0.84 mm. For one dimensional strain fields, this strain resolution can be reduced by averaging to approximately 100 με.

Thermographic Phosphor Temperature Measurement

Thermographic phosphors include rare-earth ions such as europium or dysprosium doped at low concentration into host crystals such as yttrium-aluminum-garnet (YAG), lanthanum oxysulfide (La_2O_2S), or yttrium oxide (Y_2O_3). Owing to their broadband absorption, many thermographic phosphors can be excited by non-coherent broadband ultraviolet sources with moderate power requirements. The lifetime of excited states is relatively long (1 μs - 5000 μs) thereby permitting the thermalization of the excited states, i.e., redistribution of the population of the excited states until it follows the temperature dependent Boltzmann distribution. The resultant spontaneous emission, which due to its long lifetime is called phosphorescence, presents characteristics that are temperature dependent. These characteristics may include, depending on the selected material, either increase in the phosphorescence with temperature[7] or decrease in the phosphorescence with temperature[8]. By grinding these thermographic phosphors into fine

powder and incorporating it in a binder, test surfaces can be coated with temperature sensitive paint which when illuminated by the required UV radiation emit temperature dependent phosphorescence.

One well tested thermographic phosphor, europium doped lanthanum oxysulfide ($La_2O_2S:Eu^{+3}$), was used for the present demonstration. When illuminated by UV radiation at nominally 366 nm, this complex fluoresces brightly in the visible spectrum. This spectral response is illustrated in Figure 3. The emission, unlike the absorption, of the Eu^{+3} dopant is not broadband[9]. Instead it consists of distinct lines emanating from the ^5D_j (j = 0,1,2,3) states, with each having a different temperature response. In particular, the $^5D_1$ line at approximately 537 nm is highly sensitive to temperature changes in the range of 300 - 500 K. By contrast the $^5D_0$ line at 614.5 nm is relatively insensitive to temperature in this range[8]. For surface temperature imaging, the test object is coated with a thin layer of a selected thermographic phosphor encased in a binder. The surface is then illuminated and the emitted phosphorescence is imaged by a CCD camera. This image is digitized and stored.

To spectrally separate the emission of specific transitions and from background radiation (e.g., room light), the camera is equipped with a bandpass filter. By proper selection of the bandpass filter, an image may be made to include almost exclusively emission by a temperature sensitive or a temperature insensitive transition. In addition, to further reduce unwanted background, separate images through the same filters but with the illuminating source turned off may be recorded and subtracted digitally from the phosphorescence images.

Since most of the emission and imaging parameters cannot be accurately determined, in particular, the spatial distribution of the irradiance incident on the phosphor, absolute measurements of the phosphorescence signal may be impractical. Alternatively two separate

images, one of the emission by a temperature sensitive transition and the other by a temperature insensitive transition can be recorded and each corrected by subtracting the residual background. By dividing the measured signal of each pixel of the first image by the measured signal of the corresponding pixels of the other image a purely temperature dependent distribution is obtained. This ratio can be related to temperature by calibration.

Combined Temperature and Strain Measurement

The single grid moiré and the thermographic phosphor techniques can be combined to allow measurements of strain and temperature distributions through a single port using a single light source and a single camera. In this combined technique, the sample is initially coated with a thermographic phosphor paint which can be used to obtain the temperature field. To also allow for strain measurement, the painted surface is marked by a grid. Two alternatives were explored as part of this work for marking this grid. In one alternative the phosphor was completely overcoated by a thin (<0.1 μm) layer of chromium. Lines of the chromium were then removed using photolithography and etching to expose the underlying thermographic phosphor. Alternatively, the layer of thermographic phosphor can be covered by a metallic mask having the desired grid pattern. By evaporating chromium over the mask-covered sample, a regular pattern of chromium lines was deposited over the phosphor paint. Either alternative can be used for flat samples, but only the second alternative is practical for marking grids on cylindrical or large scale samples. When the grid-covered surface is illuminated by a UV source, the exposed lines of thermographic phosphor phosphoresce while the chromium covered lines remain dark. By imaging this grid through a bandpass filter centered at the emitting phosphor line, high contrast images of the grid can be obtained.

Figure 4a illustrates the image of an alternating line array of $La_2O_2S:Eu^{+3}$ and Cr established using the photolithography technique. The illustrated 200 x 200 pixel section shows a

2.5mm × 2.5mm sample area and is magnified so the individual pixels can be distinguished. This array was illuminated by a UV light source at 366 nm, and imaged through a bandpass filter centered at 535 nm. The bright lines are due to the emission of the $^5D_0$ line of the thermographic phosphor that was exposed by etching the thin chromium layer. The image presents a high quality array of alternating chromium and thermographic phosphor lines. However, due to the crystalline morphology of the thermographic phosphor, the bright lines are non-uniform. Before a moiré pattern can be obtained, the random noise associated with this non-uniformity must be eliminated.

A new filtering algorithm was developed for removal of random noise from digitally imaged moiré and interferometric fringe patterns. In addition to effective noise removal, the filter was designed to minimize distortion of imaged geometrical shapes. This is a modification of a spin filter presented previously[10]. The algorithm defines a kernel around each pixel and detects the direction of the fringe passing through that kernel. The median grey level along this preferred direction is then used to replace the grey level recorded by the pixel at the center of the kernel. By eliminating pixels with extraneous grey levels prior to the start of the selection process, the modified filter improves the success rate of detection of the preferred direction[11]. Adverse effects of extraneous pixels are further reduced by assigning a median rather than a mean to the central pixel. Applications of the modified spin filter, the original spin filter, and of a fast Fourier transform algorithm to images of moiré patterns showed the modified spin filter to be more effective than the other filters by reducing nearly 90% of the noise and by enhancing the contrast between features of the image. At the same time, the distortion of straight moiré fringes by the modified spin filter is only 2/3 that induced by the other filters. The use of the modified spin filter was also demonstrated for processing of shadowgraph images of shockwaves.[12]

For comparison with Figure 4a, a spin filtered image is shown in Figure 4b. Clearly, both

the bright and dark grating lines now appear uniform and well defined. Moiré patterns obtained by overlapping this grating with its duplicate produce straight and evenly spaced parallel fringes.

Demonstration of Combined Temperature and Strain Measurement

The combined measurement of strain and temperature was demonstrated by imaging the temperature and thermally induced strain fields induced on an unrestrained aluminum plate on which a 1-D thermal gradient was imposed. Figure 5 shows a schematic of the apparatus including the 10.2 cm × 2.5 cm × 0.32 cm plate. A constant lengthwise temperature gradient was established near the center of this plate by heating the top with heating elements and immersing the bottom in an ice water bath. The center 2.5 cm × 2.5 cm section of the sample was coated with $La_2O_2S:Eu^{+3}$ by applying a mixture of phosphor and Sperex SP-115 Experimental Binder with an air brush and overcoating it with a thin (< 0.1 μm) Cr layer by evaporation. The chromium was then coated with photoresist, exposed through a 10 line pair/mm mask, and etched to produce the desired grid pattern. For calibration, the back side of the plate was instrumented with 5 thermocouples evenly spaced along the centerline of the prepared region. Temperatures of 423 K and 375 K were recorded at the top and bottom respectively of a 1.27 cm × 1.27 cm region at the center of this plate. Two additional thermocouples placed transverse to the center were used to monitor the transverse temperature gradient. The etched side of the plate was illuminated with a broadband lamp nominally emitting at 366 nm. Images of the center 1.27 cm × 1.27 cm section of the sample were recorded prior to and following establishment of the thermal gradient using an 8 bit CCD camera with an image resolution of 1,024 × 1,024 pixels. Images were obtained through a 535 nm and a 610 nm bandpass filter, each having a 10 nm bandwidth, and digitally stored.

Although the emission of the selected transition was separated from background radiation

(e.g., room light), by using the bandpass filters some residual background radiation could still be detected. To further reduce that background, separate images through the same filters, but without UV illumination, were recorded and subtracted digitally from the phosphorescence images. Following background subtraction, each of these images was processed by the modified spin filter using a 21 x 21 pixel kernel. Images of the grid recorded through the 535 nm filter were then divided pixel by pixel by the corresponding images obtained through the 610 nm filter, thereby correcting through normalization, effects of non-uniform coating, illumination or pixel sensitivity. For calibration purposes and to reduce effects of random noise, a horizontal average along the centerline row of each exposed phosphor line was performed for each of the phosphorescence images and a ratio of the two intensity distributions was calculated. The distribution of this averaged intensity ratio along the sample axis was then correlated with the nearly linear axial temperature distribution that was independently determined by the thermocouples. Figure 6 shows the variation of this intensity ratio in arbitrary units versus temperature. Although the projected variation is non-linear[13], the results within this narrow temperature range show nearly linear dependence. This calibration can be used for subsequent measurements when the same phosphor and same optical system are used. From the scatter between the data points the uncertainty in row averaged temperature measurements is approximately ±5 K.

To further illustrate the use of this technique, Figure 7 presents an image of the two-dimensional temperature distribution on the surface of the sample. Following background subtraction and normalization, a running average of 64 x 64 pixel groups were obtained representing a 0.8 mm x 0.8 mm spatial resolution. Using the temperature calibration curve (Fig. 6) this normalized and averaged image was transformed to the temperature field shown in

Figure 7. As expected regions of constant temperature are delineated by nearly horizontal parallel lines. Temperature uncertainty in the image is estimated to be approximately ±5 K.

Measurements of the normal strain field induced by the thermal gradient were obtained from images of the grid recorded for heated and unheated samples. A strained moiré pattern was developed by rotating a heated sample grid image by 4° and overlaying it by an unrotated image of an unheated sample. Also, a reference moiré image was generated by overlaying an unheated sample grid image with one rotated by 4°. The local fringe rotation angle, γ, was then determined from the difference in heated and unheated sample moiré fringe angle and from this the local strain was computed. To avoid temperature induced intensity variations, all images for strain measurements were obtained through the 610 nm filter.

Figure 8 illustrates the variation of the measured thermally induced strain with temperature along the sample centerline. For comparison, the strain along the centerline was also calculated using the measured coefficient-of-thermal-expansion and thermocouple temperatures and is presented as the solid line. As expected, for 1-D heating, the strain as determined by both techniques varies linearly along the centerline. The error bars were determined from predicted uncertainty in the measurement of the fringe angle. Comparison of the two data sets suggest that strain can be measured to an accuracy of $\Delta\varepsilon < \pm 250\ \mu\varepsilon$. Independent calibration measurements using a tensile test machine indicate that the lower limit of this measurement technique is approximately 100 $\mu\varepsilon$, while the upper end can be extended to sample failure.

Finally, to demonstrate the potential for imaging the distribution of strain, the variation of the thermally induced strain is presented in Figure 9. A measurement uncertainty of approximately $\pm$ 250 $\mu\varepsilon$ can be estimated from the horizontal variation in measured strain in this figure.

Conclusions

A combined strain and temperature measurement technique was demonstrated by combining a new single grid moiré interferometry technique with a thermographic phosphor technique. Images of the temperature and thermally induced strain were obtained using a single UV light source and a single camera. The incorporation of a modified spin filter to process images of the line arrays has improved the overall accuracy of strain and temperature measurement. Strain and temperature resolutions of $\Delta\varepsilon = \pm 250\ \mu\varepsilon$ and $\Delta T = \pm 5$ K with a spatial resolution of $0.8 \times 0.8\ mm^2$ were demonstrated. This technique has potential for applications to temperatures well above those of the present study. For example, YAG:Dy thermographic phosphor has been used[12] to obtain two line temperature measurements to 1700 K.

References

1. Prins, R., Laufer, G., Krauss, R. H., and Narasimhan, S., "An Optical Method for Simultaneous Measurement of Surface Strain and Temperature," *AIAA 33rd Aerospace Sciences Meeting*, AIAA 95-0482, January 1995.
2. Post D., Han, B., and Ifju P, "High Sensitivity Moiré: Experimental Analysis for Mechanics and Materials" New York: Springer Verlag, 1994.
3. Meadows, D. M., Johnson, W. O., and Allen, J. B., "Generation of Surface Contours by Moiré Patterns", *Applied Optics*, Vol. 9, 1970, pp. 942-947.
4. Durreli, A. J., and Parks, V. J., "Moiré Analysis of Strain" Prentice Hall Englewood Cliffs, New Jersey, 1970.
5. Cloud, G. L., "Optical Methods of Engineering Analysis" Cambridge University Press, New York, 1995.

6. Asundi, A., "Computer Aided Moiré Methods", *Optics and Lasers in Engineering*, Vol. 18, 1993, pp. 213-238.

7. Goss L. P., Smith A. A., and Post M. E., "Surface Thermometry by Laser-Induced Fluorescence", *Review of Scientific. Instrumentation*, Vol. 60, 1989, pp. 3702-3706.

8. Fonger W. H., and Struck C. W., "Eu^{+3} ^5D Resonance Quenching to the Charge-Transfer States in Y_2O_2S, La_2O_2S, LaOCl", *Journal of Chemical Physics*, Vol. 52, 1970, pp. 6364-6371.

9. Krauss, R. H., Hellier, R. G., and McDaniel, J. C., "Surface Temperature Imaging below 300 K using La_2O_2S:Eu, " *Applied Optics*, Vol. 33, 1994, pp. 3901-3904.

10. Yu, Q., "Spin Filter Processing and Automatic Extraction of Fringe Centerlines in Digital Interferometric Patterns", *Applied Optics*, Vol. 27, 1988, pp. 3782-3784.

11. Westring, B. W., "Simultaneous Measurement of Strain and Temperature Distributions Using Digital Imaging", Master's Thesis, University of Virginia, August 1996.

12. Laufer, G., Westring, B. D., and Marino, R. P., "Modified Spin Filter for Noise Reduction in Aerodynamic Imaging", *Optics and Laser Technology*, Vol. 29, No. 3, 1997, pp. 159-163.

13. Hellier, R., "Development of Temperature Imaging Techniques Using Thermographic Phosphors", Master's Thesis, University of Virginia, January 1992.

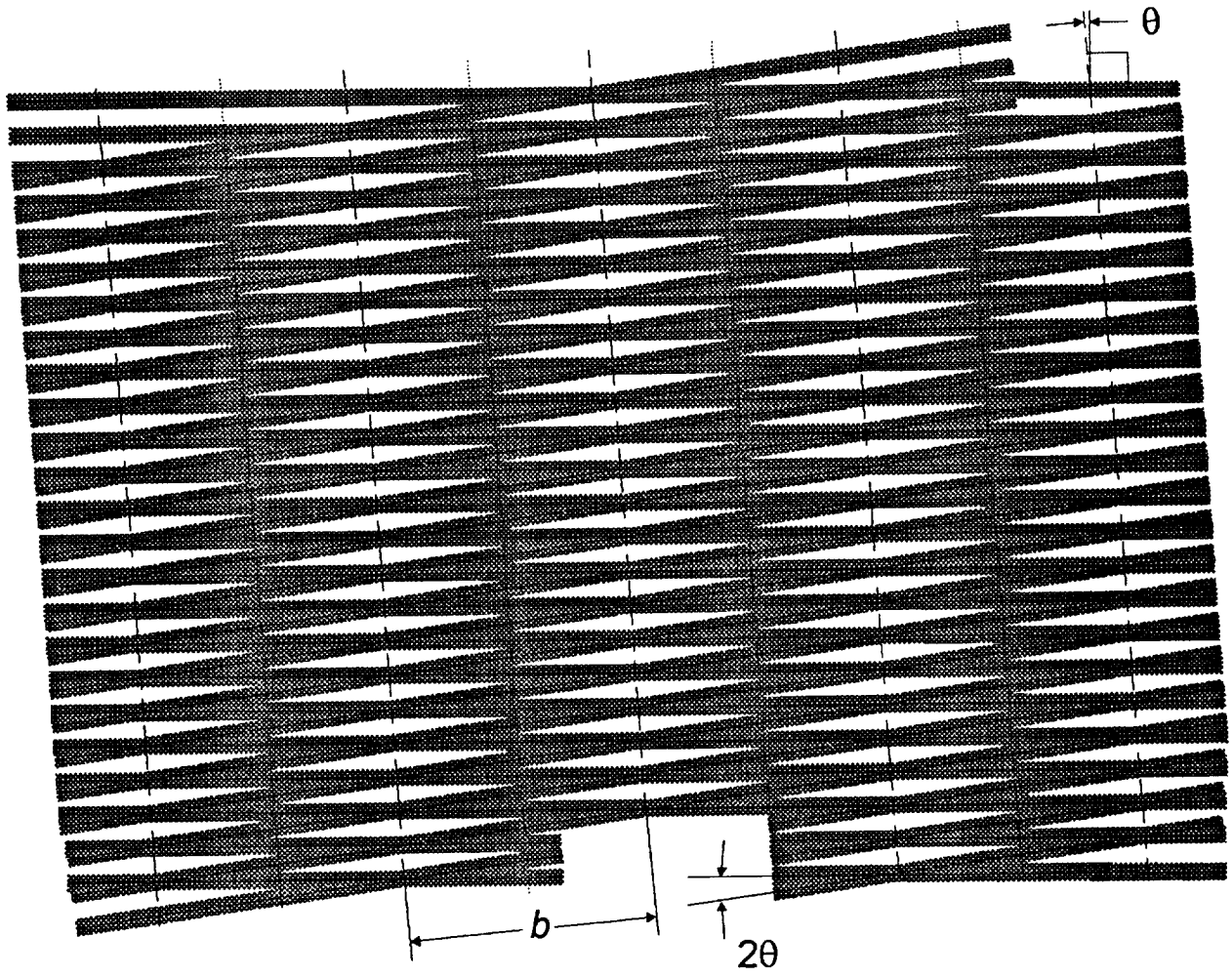

Figure 1: Moiré fringes formed from two unstrained arrays.

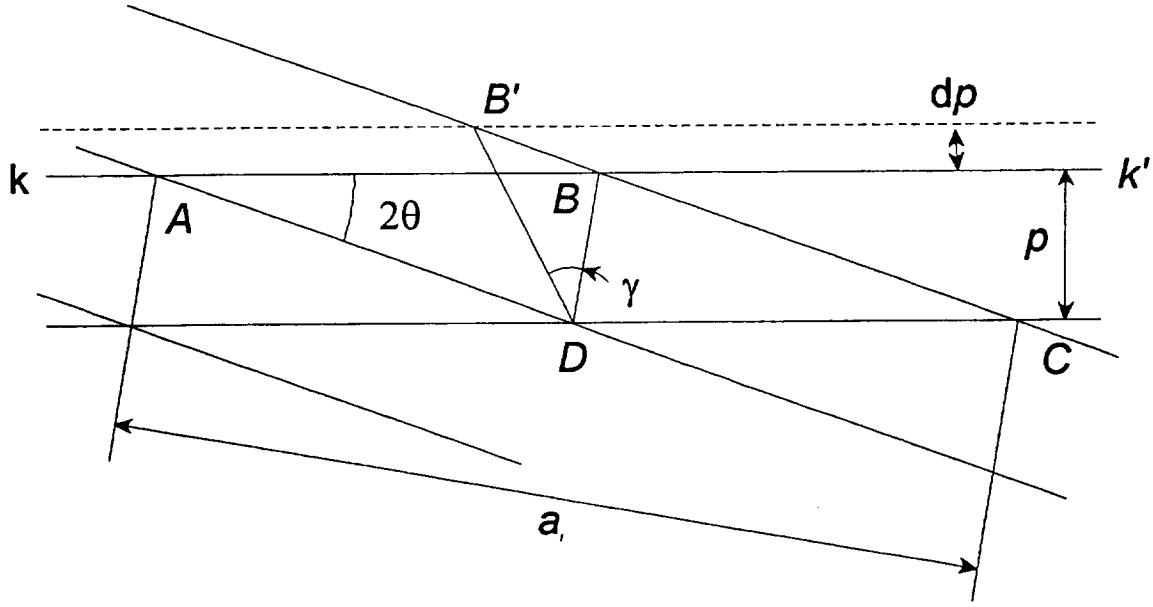

Figure 2: Geometric relationship between a reference and a strained line array.

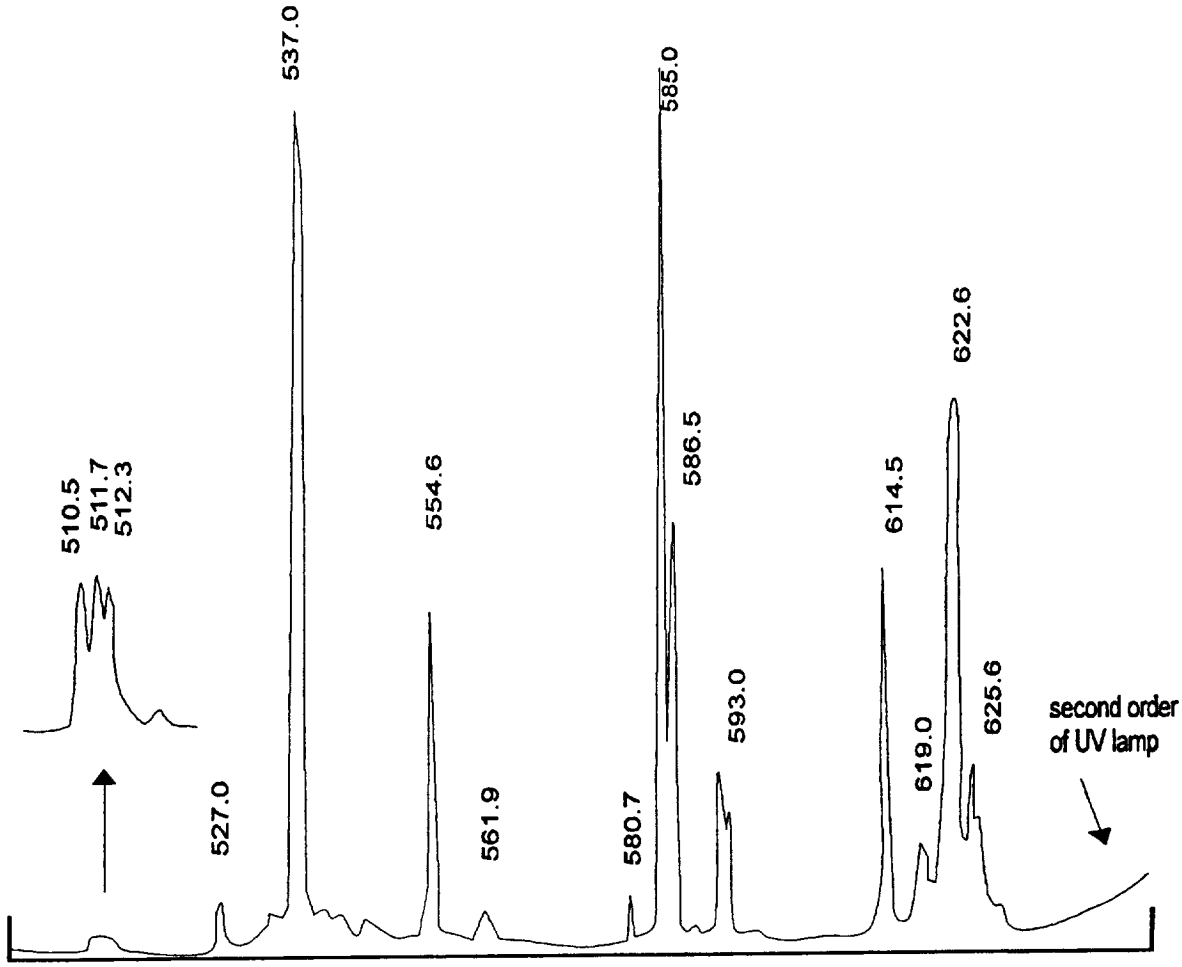

Figure 3: Emission spectrum of $La_2O_2S:Eu^{+3}$ excited by broadband UV at room temperature.

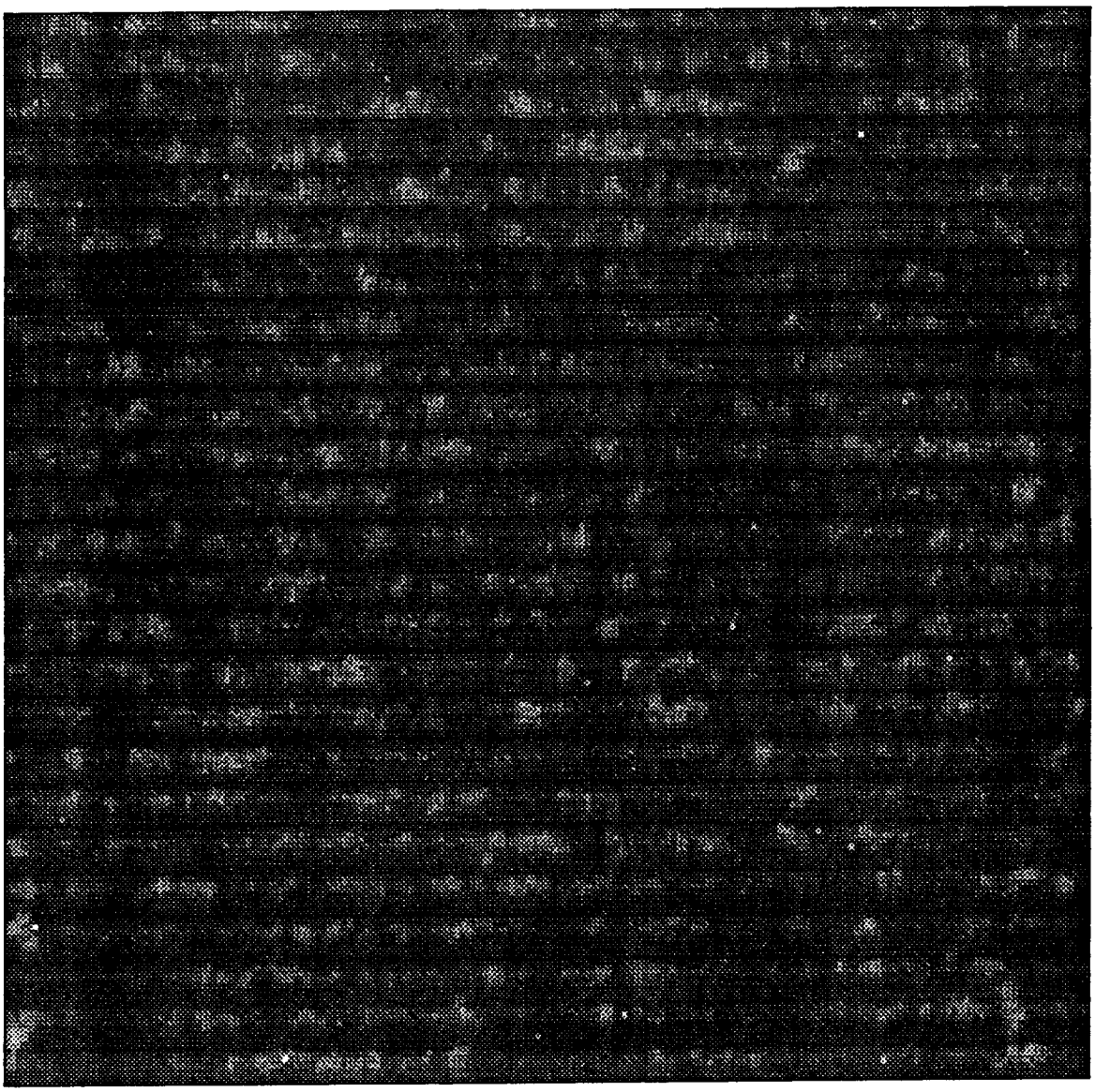

(a) Before filtering

Figure 4: Imaged line array prior to and following filtering process.

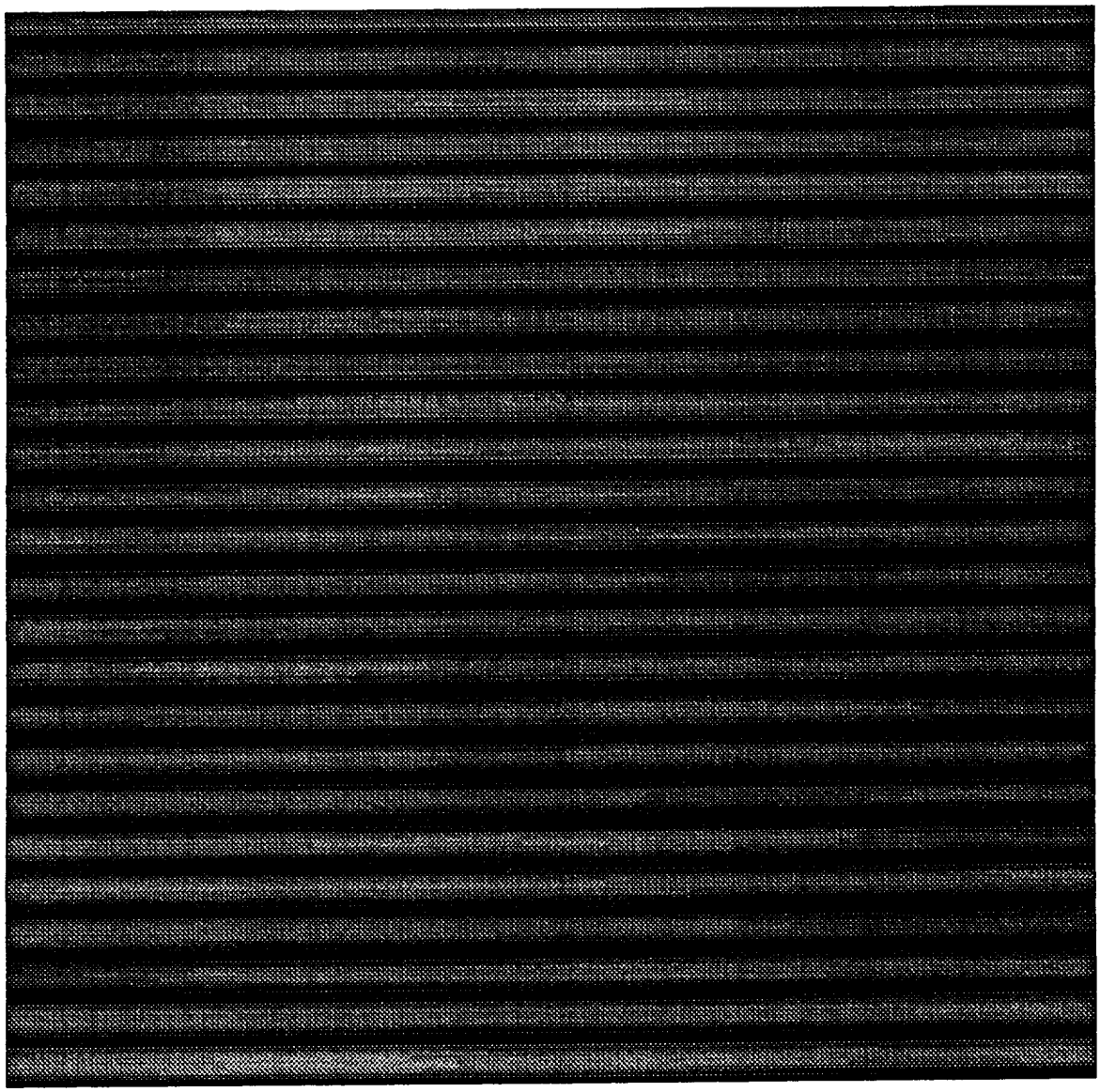

(b) After filtering

Figure 4: Imaged line array prior to and following filtering process.

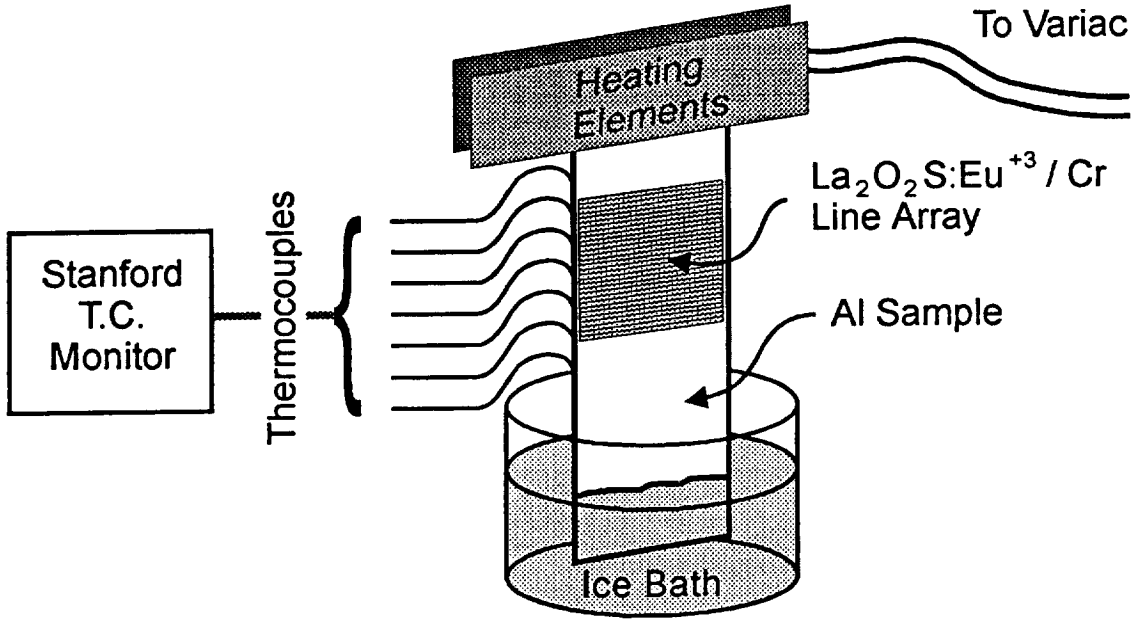

Figure 5: Schematic of 1-D temperature and thermal strain field apparatus.

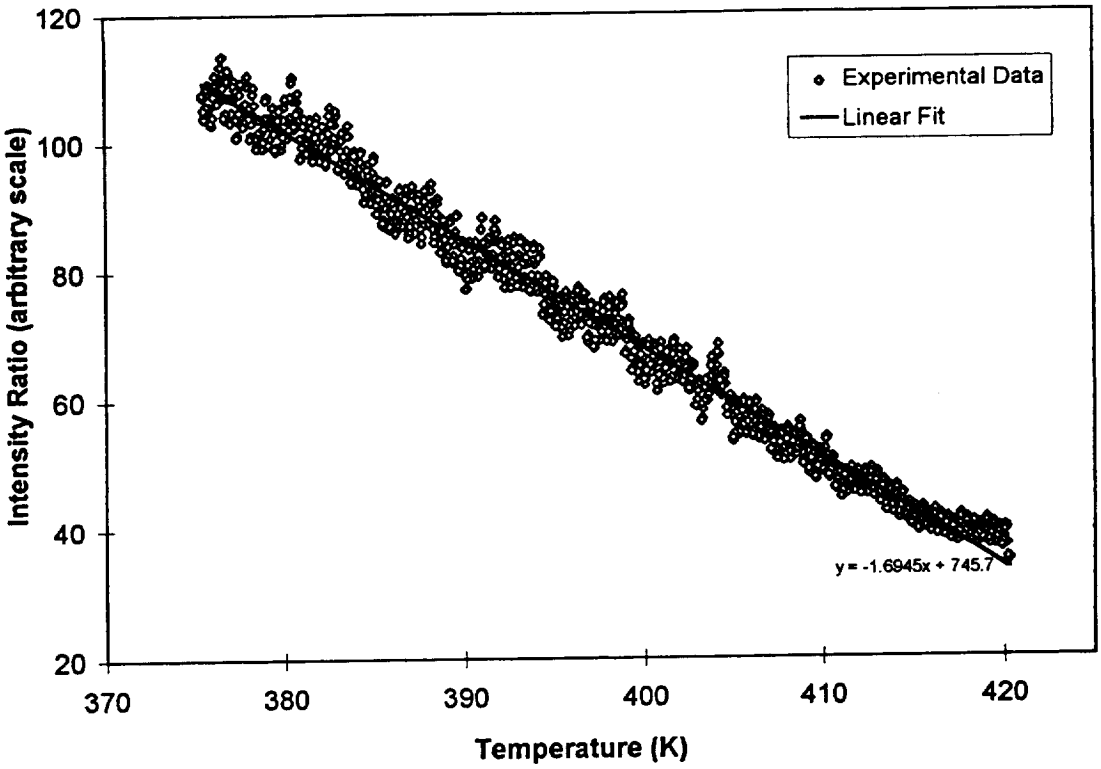

Figure 6: Normalized phosphor intensity distribution versus temperature.

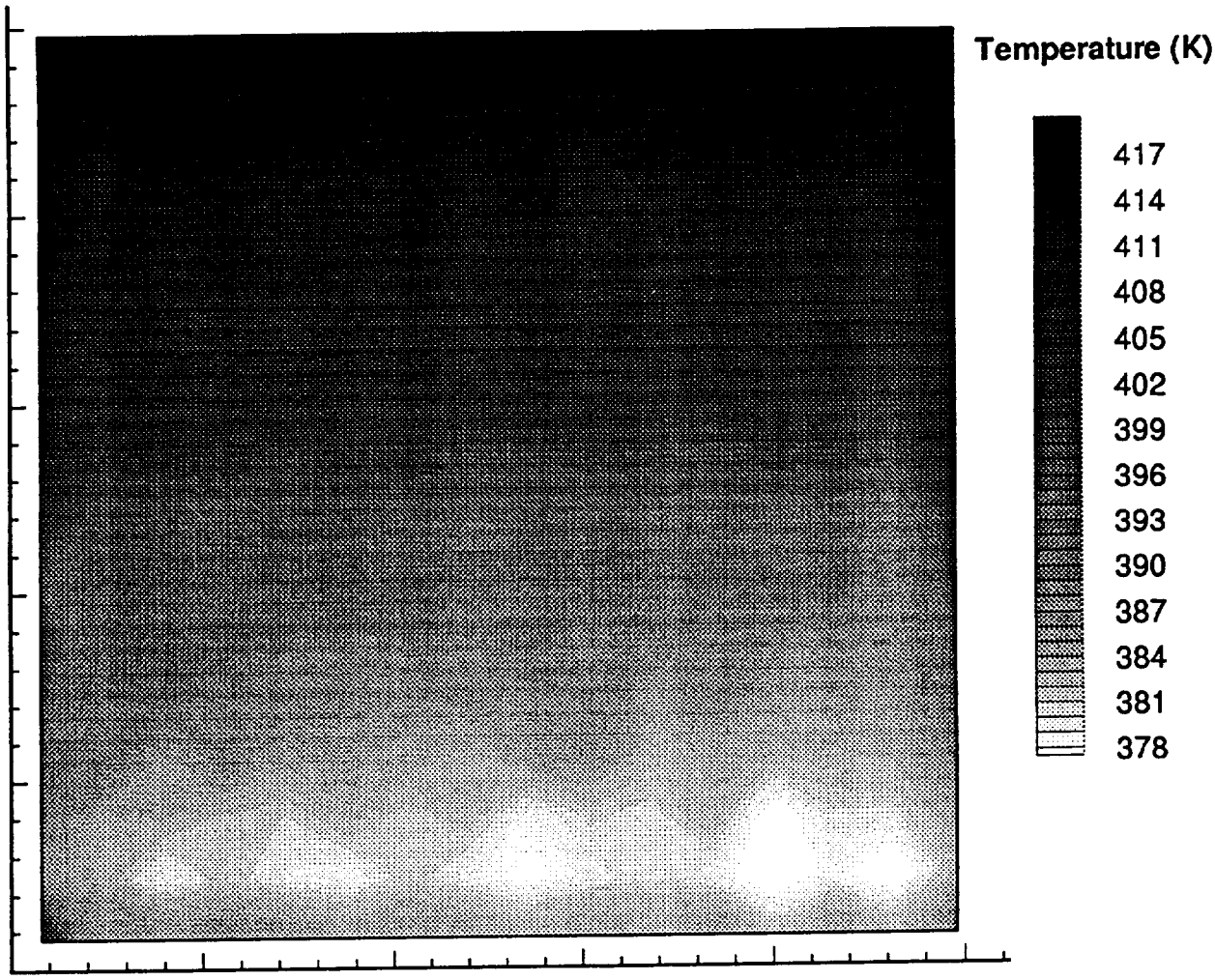

Figure 7: Temperature distribution in central 1.27 cm x 1/2 cm section of test sample.

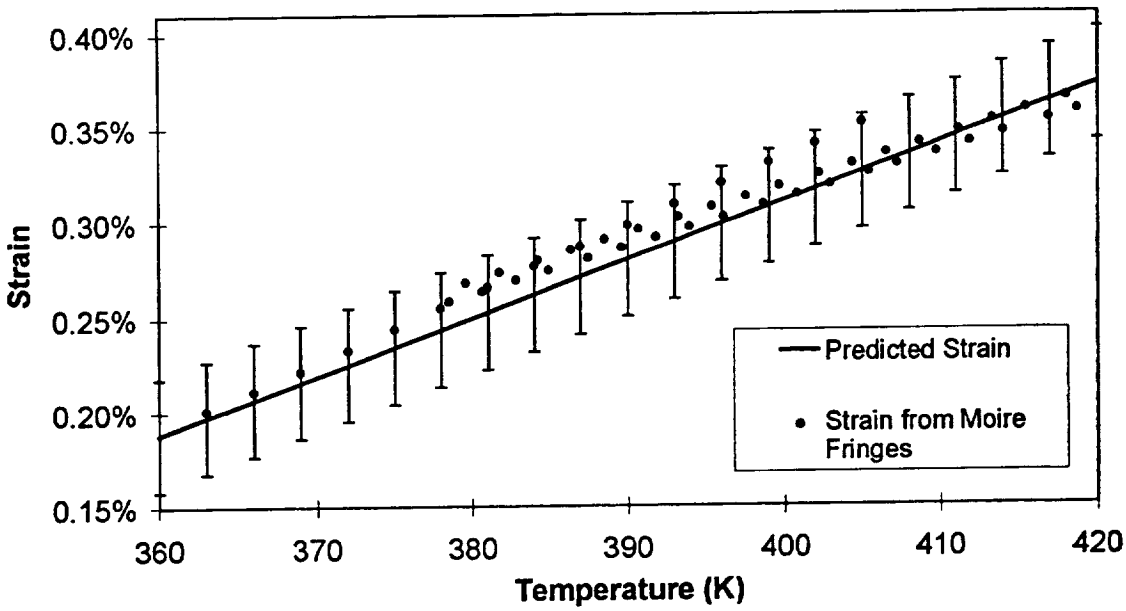

Figure 8: Comparison of imaged normal strain measurement with CTE expansion prediction.

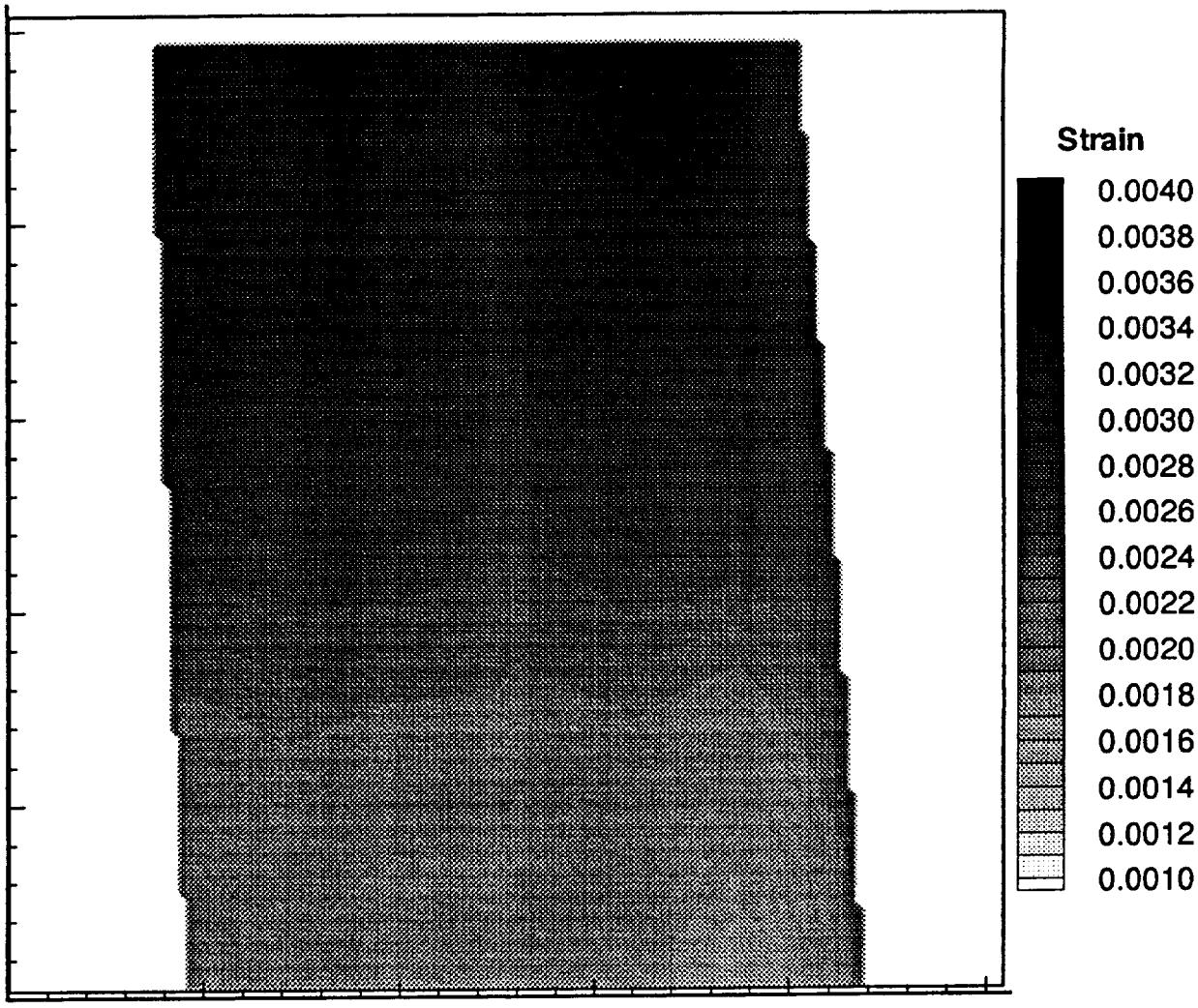

Figure 9: 2-D thermally induced strain field resulting from an imposed 1-D temperature distribution.

DISTRIBUTION LIST

1 - 3	Ms. Panice H. Clark, Grants Officer NASA Langley Research Center Acquisition Division Hampton, VA 23681-0001
4 - 5	E. A. Thornton
6	R. D. Flack, Jr.
7 - 8	SEAS Postaward Research Administration
9	SEAS Preaward Research Administration

JO#0053:ph